Naissance de la théorie quantique

Lumière : thermodynamique du rayonnement

Rayonnement de corps noir

$R(\nu;T)$ = énergie rayonnée par unité de volume et de fréquence

ν = fréquence

$\omega = 2\pi\nu$ = " angulaire

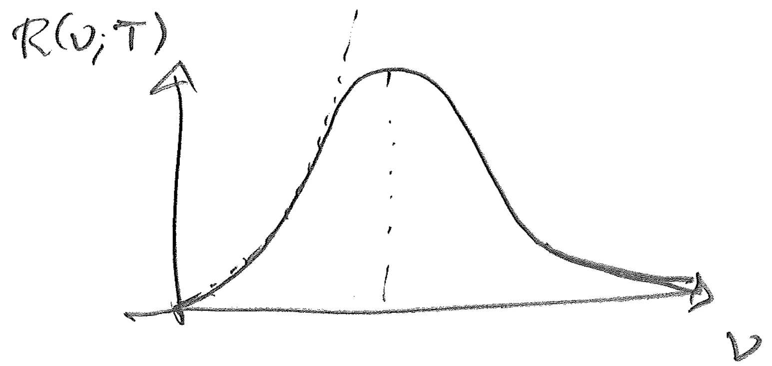

Rayleigh-Jeans (classique)

$$R(\nu,T) = \frac{8\pi\nu^2}{c^3} k_B T$$

$k_B = 1.38 \times 10^{-23}$ J/K

$c = 3 \times 10^8$ m/s

Max Planck (1900)

$$R(\nu,T) = \frac{8\pi\nu^2}{c^3} \frac{h\nu}{e^{h\nu/k_BT} - 1} \rightarrow h\nu\, e^{-\frac{h\nu}{k_BT}}$$

$$\left\{ \begin{array}{l} h = 6.62 \times 10^{-34} \text{ J}\cdot\text{s} \\ \hbar = 1.054 \times 10^{-34} \text{ J}\cdot\text{s} = \frac{h}{2\pi} \end{array} \right.$$

Constante de Planck

paquets d'énergie de $\underline{h\nu} = \epsilon$

$$\epsilon = h\nu = \hbar\omega$$

A. Einstein (1905)

"quanta de lumière" → photon

$\omega = ck$

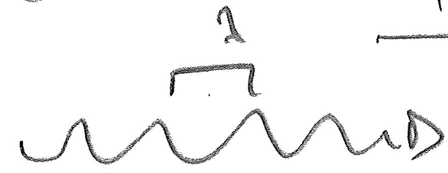

$$= \frac{2\pi c}{\lambda} \qquad k = \frac{2\pi}{\lambda}$$

$$\epsilon = \hbar\omega = \hbar c k = cp$$

$p = \hbar k$ impulsion ou quantité de mouvement

$$\epsilon = \frac{p^2}{2m} = \frac{1}{2} m v^2$$

Effet photoélectrique (1905)

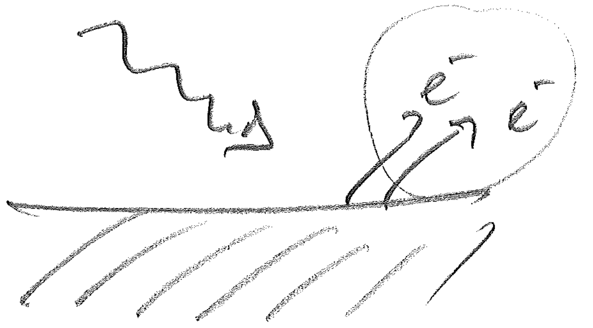

$$E_{kin}(\nu) = \alpha(\nu - \nu_0) = \alpha\nu - W$$

$\alpha \rightarrow h$

$\alpha\nu_0 = W$ "work function"

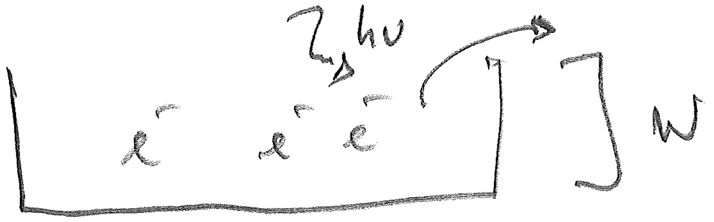

Diffusion Compton (1923)

A. Compton

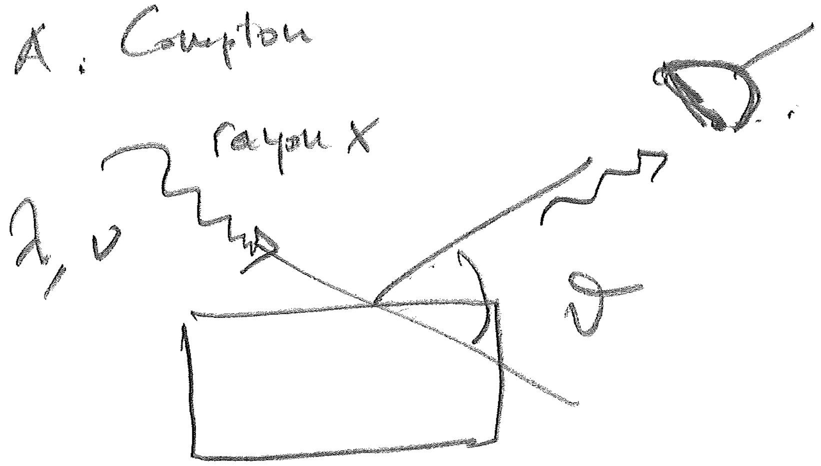

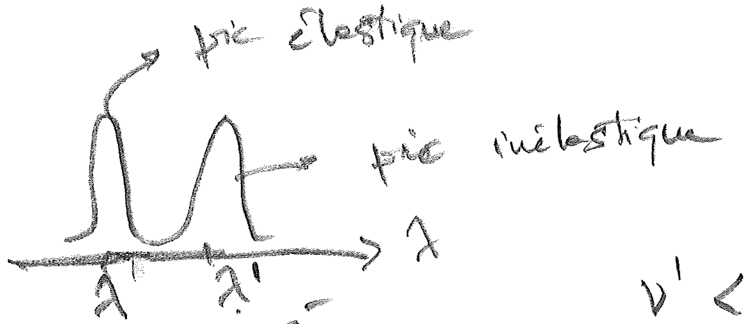

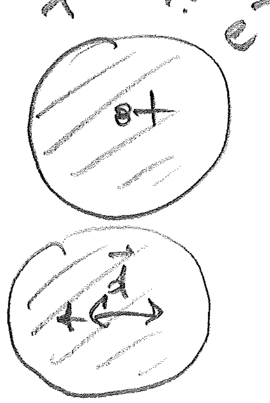

$\nu' < \nu$

$\epsilon' = h\nu' < \epsilon = h\nu$

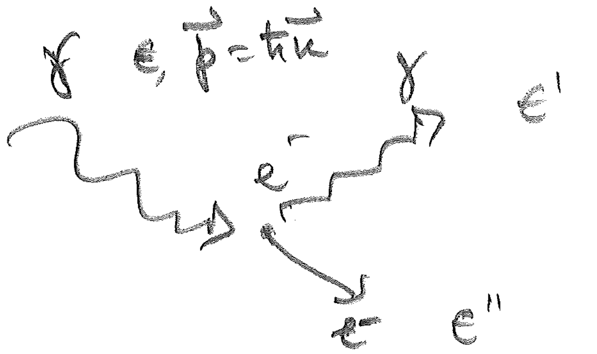

$$\epsilon' + \epsilon'' = \epsilon$$

$$\lambda' - \lambda = \lambda_c (1 - \cos\vartheta)$$

$$\lambda_c = \frac{h}{m_e c} = 2.4 \times 10^{-12}\ \text{m}$$

longueur d'onde de Compton

m_e : masse de l'électron

Dualité onde-matière

Double fente de Young

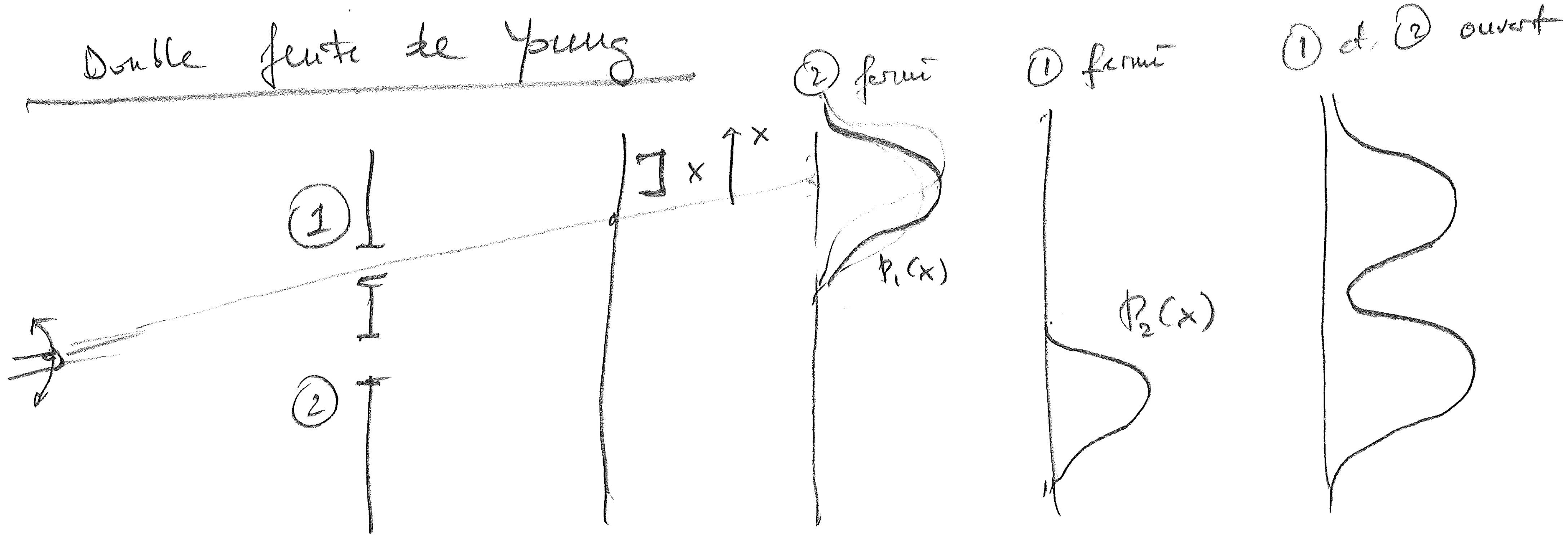

N_p projectile $\qquad \dfrac{N(x)}{N_p} \xrightarrow[N_p \to \infty]{} P(x)$

- Si j'obstrue la fente 2
- " " " " " 1

$P_{12}(x) \neq P_1(x) + P_2(x)$

$P_1(x) = P(x|1) = |A(x|1)|^2$

↳ amplitude de probabilité

$A \in \mathbb{C}$

$A(x|1) = \langle x|1\rangle$

$|1\rangle \to$ propriété de passer par 1

$|x\rangle \to$ " d'arriver en x

$$P(a\to b\to c\to d\to x) = |\langle x|d\rangle|^2 |\langle d|c\rangle|^2 |\langle c|b\rangle|^2 |\langle b|a\rangle|^2$$

Diffraction et interference d'une onde

λ, $K = \frac{2\pi}{\lambda}$

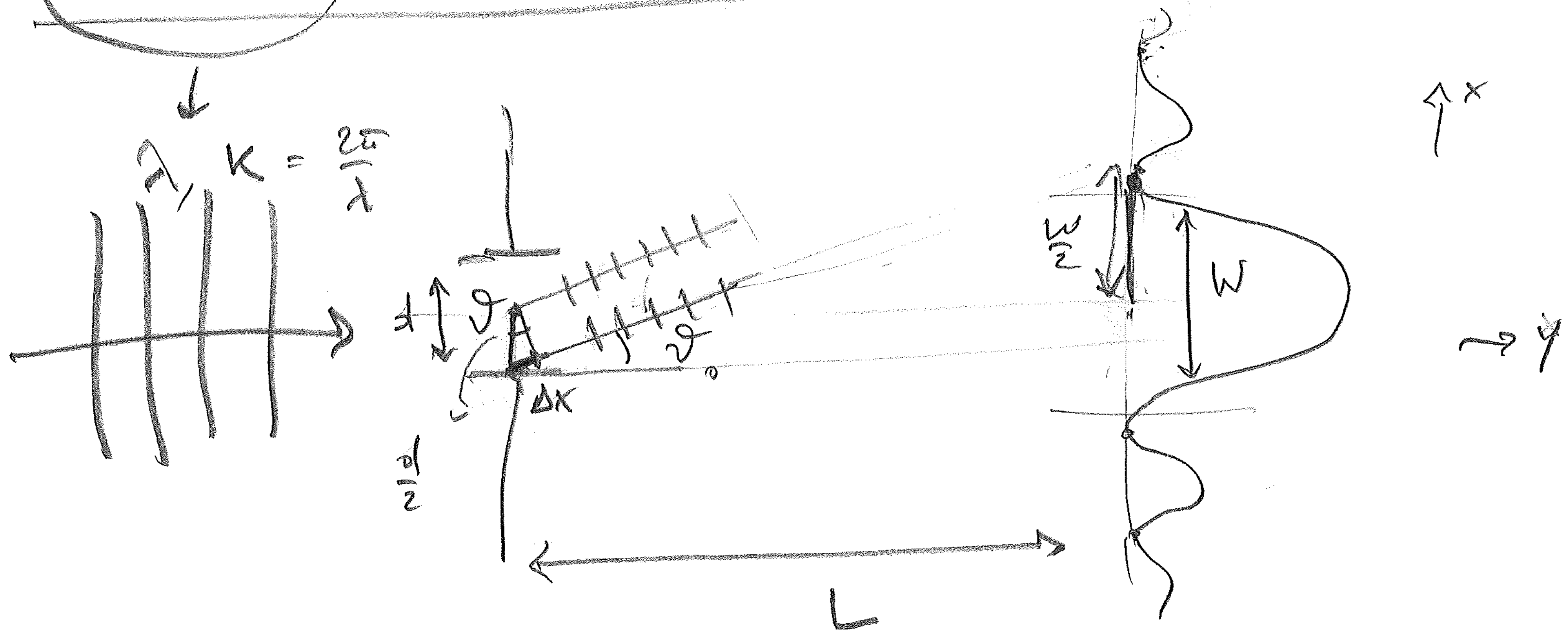

$$\Delta x = \frac{d}{2}\sin\vartheta_0 = \frac{\lambda}{2}$$

$$\sin\vartheta_0 = \lambda/d$$

$$W = 2L\sin\vartheta = 2L\frac{\lambda}{d} \qquad \frac{W}{2L} = \frac{\lambda}{d}$$

$$\vec{k} = \frac{2\pi}{\lambda}(0,1,0)$$

$$\frac{\Delta k_\perp}{k} \simeq \frac{W/2}{L} = \frac{W}{2L} = \lambda/d$$

$$k = \frac{2\pi}{\lambda}$$

$$\boxed{\Delta k_\perp \cdot d \simeq 2\pi}$$

$$\frac{\Delta k_\perp}{k} \simeq \frac{W}{2L} = \frac{\lambda}{d}$$

$$\boxed{\Delta k_\perp \cdot d \simeq 2\pi}$$

principe d'indetermination

$$\vec{k} \to \vec{k}' = (\Delta k_\perp, \underbrace{\sqrt{k^2-\Delta k_\perp^2}}_{k}, 0)$$

Double fente si (1) est ouvert si (2) est ouvert si (1) et (2) sont ouvertes

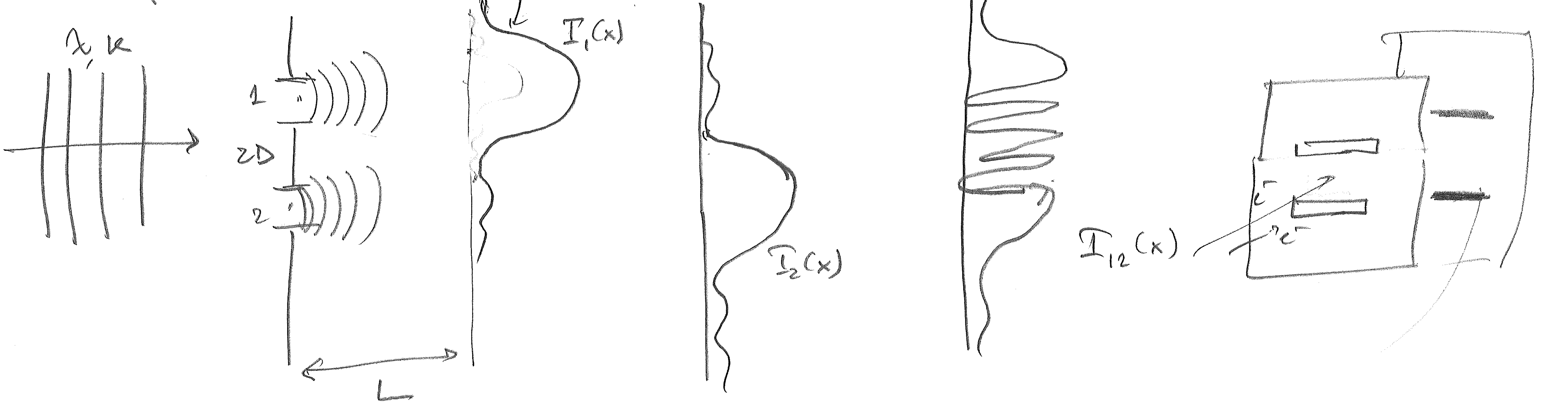

$$I_1(x) \sim |E_1(x)|^2$$

$$I_2(x) \sim |E_2(x)|^2$$

$$I_{12}(x) \sim |E_1(x)+E_2(x)|^2 \approx I_1(x)+I_2(x)+2\,\mathrm{Re}(E_1^* E_2)$$

$$\downarrow$$

$$1+\cos\left(\frac{kD}{L}x\right)$$

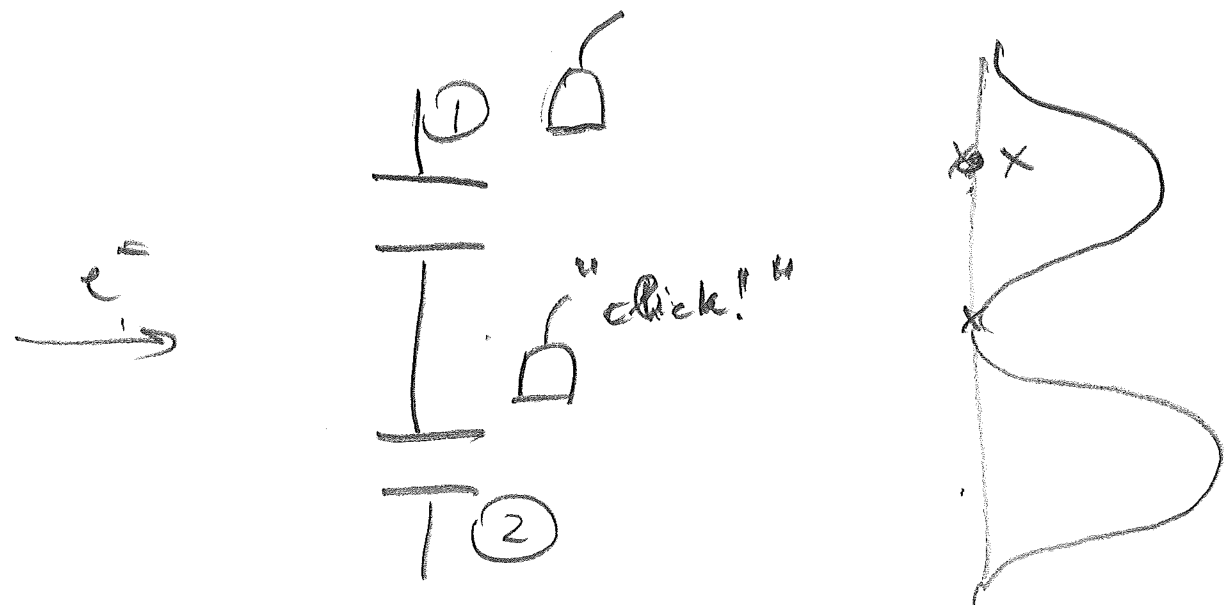

Principe de indiscernabilité

Deux processus interfèrent seulement s'ils sont indiscernables par rapport au résultat final.

Double-slit experiment

Double-slit experiment

Back to the previous page

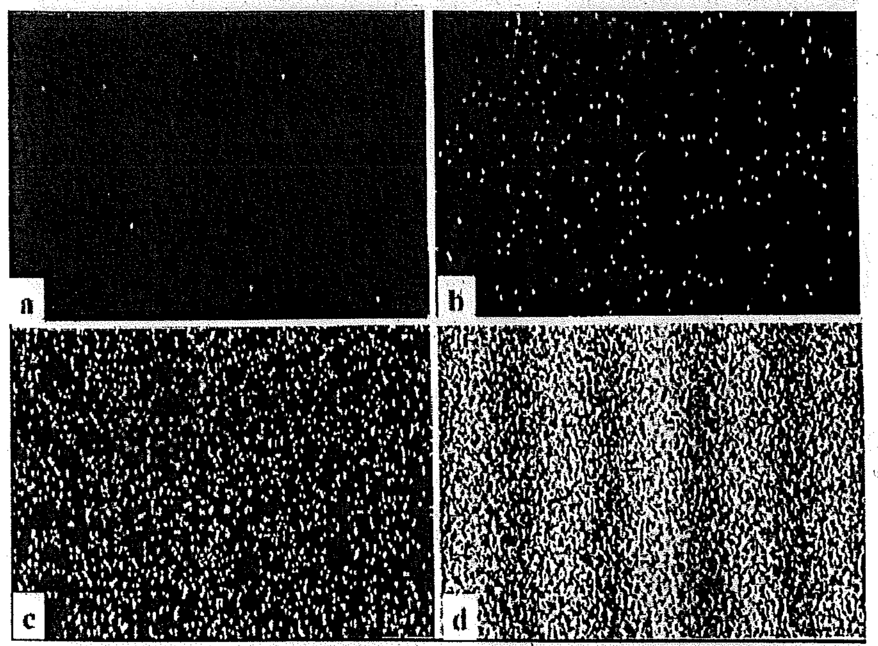

Fig. 2 Single electron events build up to from an interference pattern in the double-slit experiments.

The number of electron accumulated on the screen. (a) 8 electrons; (b) 270 electrons; (c) 2000 electrons; (d) 160,000. The total exponsure time from the beginning to the stage (d) is 20 min.

Research Areas
Research Highlights
Quantum Measurement
Verification of the Aharonov-Bohm effect
Development of the 1MV Field Emission Electron Microscope
Observations of cobalt smoke particle
Double-slit experiment
Movies
Genome Analysis
Brain Science Applications
Robotics
Next-generation Interface
Information Security

page top

Neutrons (1988)

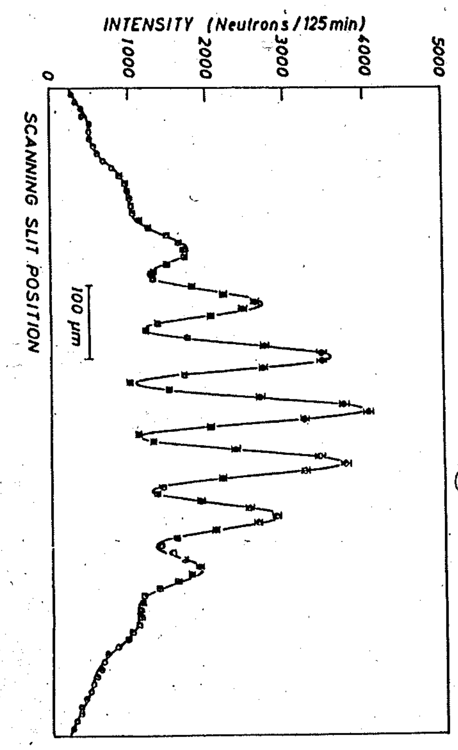

FIG. 7. Double-slit diffraction pattern. The solid curve represents the first-principles theoretical prediction. The slight asymmetry is explained by the known small unequality of the widths of the two slits.

Rev. Mod. Phys., Vol. 60, No. 4, October 1988

Atomes de Néon (1992)

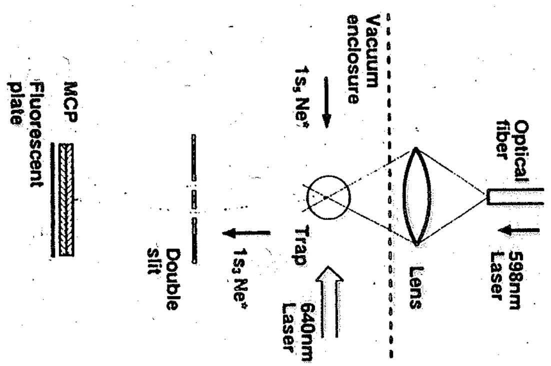

FIG. 1. Schematic experimental configuration. Details of the trap are not shown.

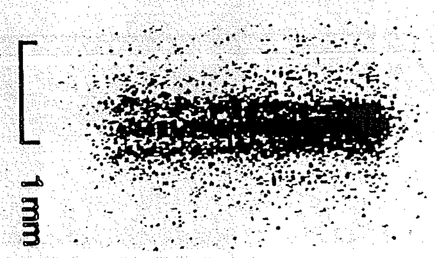

FIG. 2. The interference fringe pattern on the MCP for atoms with the initial velocity of approximately zero. The vertical length of the slit image is 2.8 mm. The spatial resolution of the picture is 20 and 32 μm for the horizontal and vertical directions, respectively. The narrowing of the fringe separation on the upper part is due to the damage of the double-slit structure. This figure contains approximately 6×10^3 atomic counts.

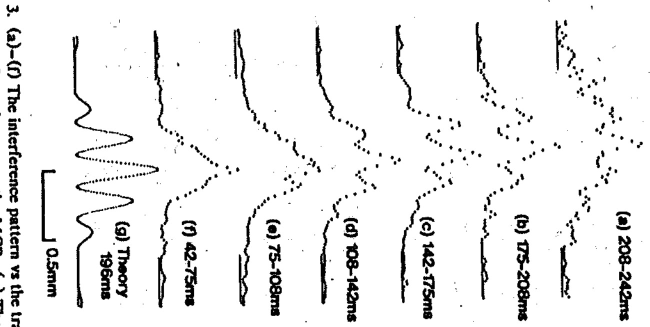

FIG. 3. (a)–(f) The interference pattern vs the transit time t of the $1s_3$ atom from the trap to the MCP. (g) The calculated pattern for $v_0=0$ m/s.

Fullérène -C60 (1999)

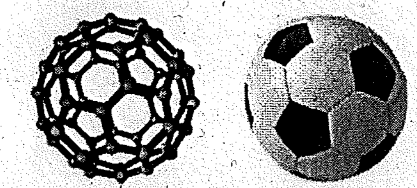

Fig. 2. The fullerene molecule C_{60}, consisting of 60 carbon atoms arranged in a truncated icosahedral shape, is the smallest known natural soccer ball.

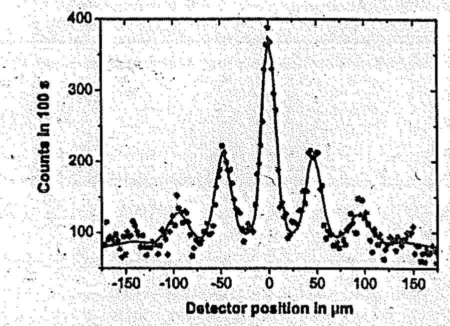

Fig. 7. Far-field diffraction of C_{60} using the slotted disk velocity selector. The mean velocity was $\bar{v}=117$ m/s, and the width was $\Delta v/v \sim 17\%$. Full circles represent the experimental data. The full line is a numerical model based on Kirchhoff–Fresnel diffraction theory. The van der Waals interaction between the molecule and the grating wall is taken into account in form of a reduced slit width. Grating defects (holes) additionally contribute to the zeroth order.

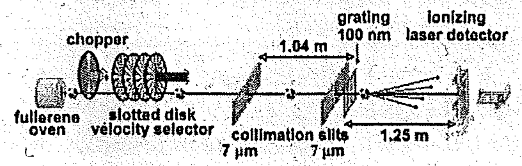

Fig. 3. Setup of the diffraction experiment. Fullerene molecules are sublimated in the oven at 900 K. The spectral coherence can be improved using a mechanical velocity selector. Two collimating slits improve the spatial coherence and limit the angular spread of the beam to smaller than the expected diffraction angle. A SiN grating with a 100 nm period and 50 nm openings is used to diffract the incident molecular waves. The molecular far-field distribution is observed using a scanning laser-ionization detector.

Grandes molécules organiques (2011)

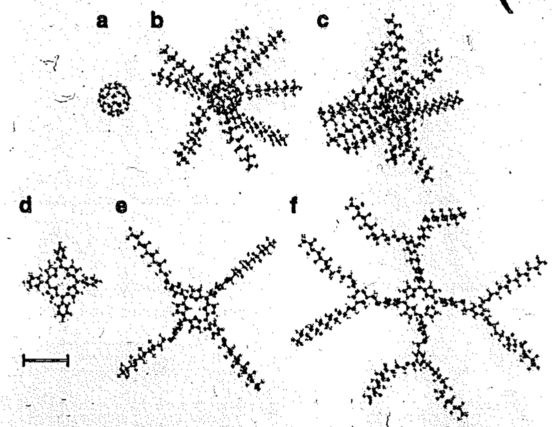

Figure 1 | Gallery of molecules used in our interference study. **(a)** The fullerene C_{60} (m = 720 AMU, 60 atoms) serves as a size reference and for calibration purposes; **(b)** The perfluoroalkylated nanosphere PFNS8 ($C_{60}[C_{12}F_{25}]_8$, m = 5,672 AMU, 356 atoms) is a carbon cage with eight perfluoroalkyl chains. **(c)** PFNS10 ($C_{60}[C_{12}F_{25}]_{10}$, m = 6,910 AMU, 430 atoms) has ten side chains and is the most massive particle in the set. **(d)** A single tetraphenylporphyrin TPP ($C_{44}H_{30}N_4$, m = 614 AMU, 78 atoms) is the basis for the two derivatives **(e)** TPPF84 ($C_{84}H_{26}F_{84}N_4S_4$, m = 2,814 AMU, 202 atoms) and **(f)** TPPF152 ($C_{168}H_{94}F_{152}O_8N_4S_4$, m = 5,310 AMU, 430 atoms). In its unfolded configuration, the latter is the largest molecule in the set. Measured by the number of atoms, TPPF152 and PFNS10 are equally complex. All molecules are displayed to scale. The scale bar corresponds to 10 Å.

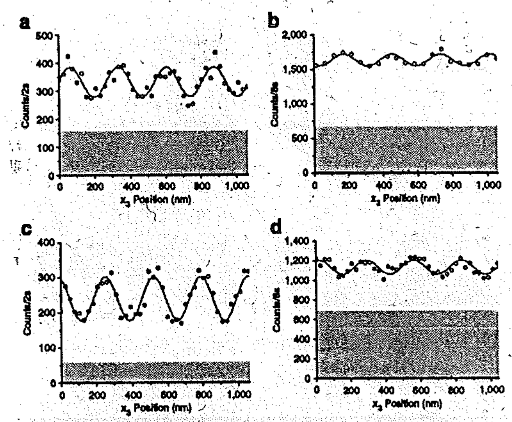

Figure 3 | Quantum interferograms of tailor-made large organic molecules. Quantum interference well beyond the classical expectations has been observed for all molecules in the set. In all panels, the black circles represent the experimental result, the blue line is a sinusoidal fit to the data and the shaded area indicates the detector dark rate. **(a)** The beam of perfluoroalkylated nanospheres, PFNS8, is characterized by a mean velocity of $v = 63\,\mathrm{m\,s^{-1}}$ with a full width $\Delta v_{FWHM} = 13\,\mathrm{m\,s^{-1}}$. The observed contrast of $V_{obs} = 49 \pm 6\%$ is in good agreement with the expected quantum contrast of $V_{quant} = 51\%$ and is clearly discernible from the classically expected visibility of $V_{class} < 1\%$. The stated uncertainty is the standard deviation of the fit to the data. **(b)** For PFNS10, the signal was too weak to allow a precise velocity measurement and quantum calculation. The oven position for these particles, however, limits the molecular velocity to $v < 80\,\mathrm{m\,s^{-1}}$ and therefore allows us to define an upper bound to the classical visibility. **(c)** For TPPF84, we measure $v = 95\,\mathrm{m\,s^{-1}}$ with $\Delta v_{FWHM} = 34\,\mathrm{m\,s^{-1}}$. This results in $V_{obs} = 33 \pm 3\%$ with $V_{quant} = 30\%$ and $V_{class} < 1\%$. **(d)** The signal for TPPF152 is equally low compared with that of PFNS10. For this compound we find $V_{obs} = 16 \pm 2\%$, $V_{quant} = 45\%$ and $V_{class} = 1\%$.

6

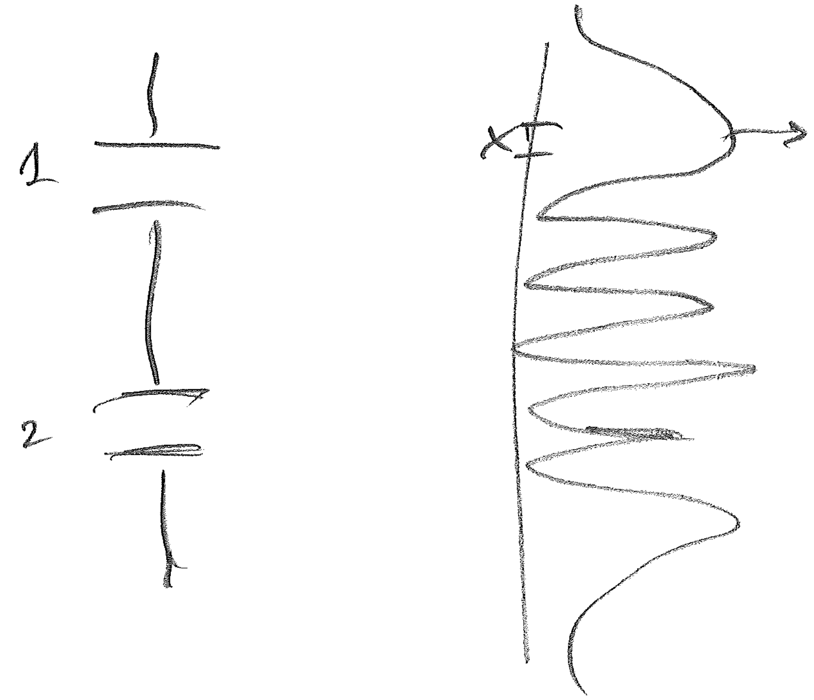

$P(x) \neq P_1 + P_2$ $\qquad P_1 = |A(x|1)|^2$

$$P_{12}(x) = |A(x|1) + A(x|2)|^2$$

$$= |\langle x|1\rangle + \langle x|2\rangle|^2$$

$k = k(E)$

L. de Broglie (1924)

$\epsilon = cp = c\hbar k$

$\omega = ck$

$p = \hbar k = \hbar \frac{2\pi}{\lambda} = \frac{h}{\lambda}$

$E = \epsilon = \frac{p^2}{2m}$

$E \to p \to \boxed{\lambda = \frac{h}{p}}$ longueur d'onde de de Broglie

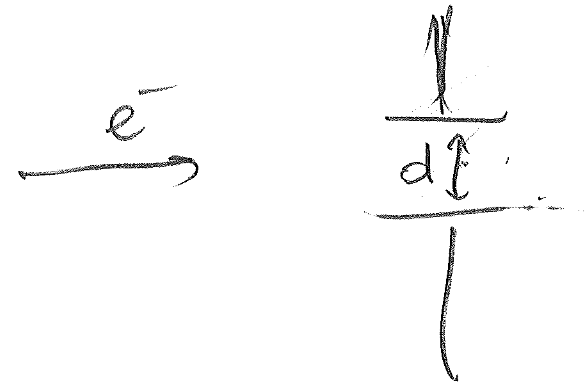

$\Delta k_\perp \cdot d \simeq 2\pi$

$\boxed{\Delta p_\perp \cdot d \simeq h}$

principe d'indétermination ou incertitude
d'Heisenberg